Development of tailored and self-mineralizing citric acid-crosslinked hydrogels for *in situ* bone regeneration

Aitor Sánchez-Ferrero[a,b], Álvaro Mata[c], Miguel A. Mateos-Timoneda[a,b], José C. Rodríguez-Cabello[b,d], Matilde Alonso[b,d], Josep Planell[a], Elisabeth Engel[a,b]*

[a]Biomaterials for regenerative therapies group, Institute for Bioengineering of Catalonia (IBEC), Barcelona, 08028, Spain.

[b]Biomedical Research Networking center in Bioengineering, Biomaterials, and Nanomedicine (CIBER-BBN), Spain

[c]School of Engineering & Materials Science, Queen Mary, University of London, London, E1 4NS, UK

[d]G.I.R. Bioforge, University of Valladolid, Valladolid, 47001, Spain

*Corresponding author. Email: eengel@ibecbarcelona.eu. Tel.: +34934020210. Fax: +34934039702

Abstract

Bone tissue engineering demands alternatives overcoming the limitations of traditional approaches in the context of a constantly aging global population. In the present study, elastin-like recombinamers hydrogels were produced by means of carbodiimide-catalyzed crosslinking with citric acid, a molecule suggested to be essential for bone nanostructure. By systematically studying the effect of the relative abundance of reactive species on gelation and hydrogel properties such as functional groups content, degradation and structure, we were able to understand and to control the crosslinking reaction to achieve hydrogels mimicking the fibrillary nature of the extracellular matrix. By studying the effect of polymer concentration on scaffold

mechanical properties, we were able to produce hydrogels with a stiffness value of 36.13±10.72 kPa, previously suggested to be osteoinductive. Microstructured and mechanically-tailored hydrogels supported the growth of human mesenchymal stem cells and led to higher osteopontin expression in comparison to their non-tailored counterparts. Additionally, tailored hydrogels were able to rapidly self-mineralize in biomimetic conditions, evidencing that citric acid was successfully used both as a crosslinker and a bioactive molecule providing polymers with calcium phosphate nucleation capacity.

Keywords

Biomimetic material; Biomineralisation; Bone tissue engineering; Cross-linking; Hydrogel; Mesenchymal stem cell

1. Introduction

Biomimicry has become the cornerstone of bone tissue engineering strategies involving the use of scaffolds. The extracellular matrix (ECM) is the tissue-specific [1] nanofibrillar platform supporting cells and regulating their behavior *in vivo* [2]. Thus, it is the archetype for the design of materials aiming to recapitulate skeletal development and to ultimately achieve tissue regeneration. Matrix properties such as structure [3], stiffness [4], surface chemistry [5], and ligand nature [6] have proved useful in promoting the osteoblastic differentiation of mesenchymal stem cells (MSCs). However, combinatorial studies [7,8] suggest their synergistic effect must be considered, evidencing that complex scaffold designs are required to more accurately direct cell behavior.

The soft and tailorable nature of hydrogels make them an ideal platform to induce bone formation by providing cells with combined ECM-mimicking signals while being remodeled and

degraded. Among the many polymers suitable to produce hydrogels, elastin-like recombinamers (ELRs) stand out as a powerful tool given their recombinant nature. This confers them great versatility regarding the inclusion of particular sequences to control processes such as cell adhesion [9], mineralization [10] and degradation [11]. Although ELRs inherit elastin's reversible self-aggregation capacity, covalent crosslinking is required to produce stable hydrogels. The crosslinking conditions used to prepare hydrogels influence their structure and mechanical properties [12], so crosslinking is a useful tool to achieve hydrogels with tuned properties.

Water-soluble carbodiimide (WSC) is a non-integrative crosslinker widely used to produce protein-based hydrogels. It catalyzes the formation of peptide bonds by condensation of primary amines ($–NH_2$) and carboxyl groups (-COOH) [13] and can be easily washed out from scaffolds, thus minimally compromising cytocompatibility. Although ELRs have been designed to include lysine residues as a source of $–NH_2$, they are short on -COOH, so carboxyl-donor molecules are required to achieve the carbodiimide-catalyzed crosslinking of ELRs. Donor molecules, ideally polycarboxylic acids such as citric acid, would then be incorporated into the polymeric matrix and might potentially provide hydrogels with new functionalities.

Up to the 80% of citric acid in the human body is found in bones [14]. This tricarboxylic acid, long known for its central role in cell metabolism, has been recently suggested to play a critical role in limiting the growth of hydroxyapatite (HA) crystals *in vivo* [15]. Conversely, citrate has been shown to induce the *in vitro* nucleation of HA on collagen matrices [16]. The presence of HA at a surface level provides scaffolds with bone regenerative potential [17], as evidenced by both *in vitro* [18] and *in vivo* [19] studies involving the use of premineralized hydrogels. Thus,

calcium phosphate-nucleation capacity is an interesting feature to boost the osteogenic potential of biomimetic hydrogels.

The goal of this study was to develop tailored citric acid-crosslinked ELRs hydrogels for in situ bone regeneration. Different crosslinking parameters were used to decipher their contribution to scaffolds' architecture, stiffness, degradation and cytotoxicity, and to ultimately extrapolate the proper set of conditions needed to achieve structurally and mechanically-tailored hydrogels. Polymeric matrices with tuned properties were assessed to determine their capacity to support cell growth, to induce the osteogenic differentiation of hMSCs and to self-mineralize in vitro. Interestingly, our results show that herein developed crosslinking reaction is a versatile and useful tool to both tune hydrogel physical properties and provide polymers with calcium phosphate nucleation capacity, thus avoiding the need of performing functionalization, in the development of scaffolds for bone regeneration.

2. Materials and methods

2.1. HRGD6 ELR

HRGD6 ELR was synthesized as previously reported [20]. This recombinant polymer, based on the repetition of VPGxG (where x is either I or K) elastomeric domains, includes lysine residues as a source of ε-NH_2 groups to be used for crosslinking purposes and RGD tripeptides for cell adhesion.

2.2. Sample preparation

HRGD6 polymer was crosslinked with citric acid monohydrate (Sigma) through a N-(3-Dimethylaminopropyl)-N'-ethylcarbodiimide (EDC, Aldrich)-catalyzed reaction in 2-(N-Morpholino)ethanesulfonic acid (MES, Sigma). Seven different hydrogels, each one characterized by a particular combination of EDC:COOH and COOH:NH_2 molar ratios, were

prepared (Fig. 1b). Setups were encoded in the form EXCY, where EX denotes the molar excess (X) of EDC with respect to –COOH groups and CY denotes the molar excess (Y) of -COOH with respect to -NH_2 groups. In all cases, HRGD6 polymer was dissolved overnight at 4ºC in MES buffer containing citric acid; similarly, EDC was dissolved overnight at 4ºC in MES buffer. Polymer-citrate and EDC solutions were mixed at a 1:1 volume ratio (polymer concentration: 40 mg/ml) and pH was adjusted to ≈ 6 by adding cold NaOH or HCl (Panreac). Crosslinking reactions were carried out at 37°C for 1 h and stopped by incubation with 0.1 M Na_2HPO_4 (Sigma) at room temperature for 3 hours. Samples were then washed by performing 5 swelling/shrinking incubation cycles in ultrapure water at 4°C (swelling)/37°C (shrinking) to allow excess EDC and reaction by-products to be released.

2.3. Effect of reaction conditions on the crosslinking reaction

2.3.1. Gelation

Reaction mixes for all seven different hydrogels were prepared as previously stated and poured into 96-well plates. Absorbance evolution was monitored at 37°C and λ=750 nm for 62.5 minutes using an Infinite M200 Pro multimode reader and i-control software (Tecan, Switzerland). Collected data were treated with Origin (OriginLab, version 8.0724); latency time, herein defined as the time lapse between the mixture of reagents and the initial increase in turbidity, was calculated using the Spectroscopy Peak Analyzer tool in Origin.

2.3.2. Quantification of unreacted –NH_2 groups

Hydrogels were prepared in 96-well plates and incubated with 100 µl of a 10.55 mM 2,4,6,-trinitrobenzenesulfonic acid (TNBS, Sigma) solution in 9:1 0.1 M $NaHCO_3$: 0.1 M Na_2CO_3 (pH 8.93) in the dark at 4°C with gentle stirring for 30 hours. 200 µl of 6 M HCl were added to completely hydrolyze samples over a 75 hours period and resulting solutions were diluted 1/10 in

ultrapure water. Absorbance was read at λ=342 nm and glycine was used to prepare standard curves to stoichiometrically quantify unreacted primary amines.

2.4. Effect of reaction conditions on hydrogels properties

2.4.1. Hydrogels structure and polymer-occupied volume

Hydrogels structure was assessed by confocal microscopy and Field Emission Scanning Electron Microscopy (FESEM). Samples to be assessed by confocal microscopy were prepared on 16-well glass chamber slides and stained with 0.4% Trypan blue (Sigma) for 3 hours at room temperature. Several washing steps with phosphate-buffered saline (PBS; Life technologies) were performed until no apparent dye release was noticed. Samples were then treated with fixative solution (3% paraformaldehyde and 40 mM sucrose in PBS; reagents from Sigma) for 10 minutes at 4°C and washed three times with cold 0.15% glycine in PBS (PBS-gly). Hydrogels were then mounted with Mowiol 40-88 (Sigma-Aldrich) and sealed with nailpolish. Images were acquired at an emission wavelength range of 579-657 nm and a stepsize of 80 nm by using a TCS SP5 confocal microscope (Leica, Germany) and LAS-AF software (Leica; version 2.4.1 build 6384). The size of polymer aggregates was measured with Fiji [21].

Hydrogels to be observed by FESEM were prepared in PDMS molds, washed with water several times to remove salts, lyophilized and sputtered with graphite. FESEM images were obtained by using a NOVA NANOSEM 230 microscope (FEI, United States) at a 3.00 kV voltage and 5 mm working distance.

Sections obtained by confocal microscopy were used to quantify the percentage of polymer-occupied volume (i.e. polymer volume/total volume; PV/TV) by using the Volume Fraction tool (BoneJ [22] plugin v.1.3.11 for Fiji). Calculations were performed with a surface resampling

value of 2 and a specific threshold for each set of images. 3D reconstructions of quantified volumes were analyzed to assure proper thresholding was used for each single calculation.

2.4.2. Resistance to enzymatic degradation

Selected samples were prepared in 96-well plates and incubated with $2.82 \cdot 10^{-3}$ U/ml porcine pancreatic elastase (Worthington Biochemical Corporation, United States) in PBS at 37ºC for 1, 3 and 7 days. Hydrogels not exposed to elastase were used to set sample weight at day 0. At every time point, samples were washed with ultrapure water, dried at 37ºC and weighted.

2.4.3. Surface stiffness

Samples were prepared in 6 mm-diameter PDMS molds and kept in PBS at 37°C until use. Molds were mounted on glass slides using double-sided tape and ten force curves per sample were acquired in Force Mode using IGOR Pro sofware (Wavemetrics, version 6.2.2.2A) and a MFP-3D stand alone unit (Asylum Research, United States). Measurements were made in PBS at 37°C using chromium and gold-coated, pyramidal silicon nitride cantilevers (NanoWorld) with a nominal spring constant of 0.08 N/nm and assuming Poisson's ratio to be 0.5. A custom-made script considering cone-shaped tip was used to calculate Young's modulus by means of Hertz model.

2.5. Effect of reaction conditions on hydrogels cytotoxicity and RGD integrity

2.5.1. Cytotoxicity

Bone marrow-derived rat MSCs (rMSCs) were cultured in 75 cm^2 flasks at 37°C in a 5% CO_2 atmosphere. Cell expansion was carried out in complete medium: Advanced Dulbecco's modified Eagle's medium (AdvDMEM; Gibco) supplemented with 15% fetal bovine serum (FBS; Gibco), 2 mM L-glutamine (Gibco), 100 U/ml Penicillin and 100 µg/ml Streptomycin (Gibco). Cells at passage 6-8 were detached at a confluence of about 80% with Tryp-LE Express

(Gibco) and the number of viable cells was determined after staining with Trypan blue. 10^4 viable cells/well were seeded on 24-well plates and allowed to adhere for 4 hours. Non-adhered cells were washed out with PBS and attached cells were quantified with 10% Alamar blue (TREK Diagnostic Systems) in complete medium to verify homogenous adhesion in all wells. Cells were then washed with PBS and wells were subsequently replenished with complete medium.

Selected hydrogels were tested for cytotoxicity by indirect contact. Samples prepared in PDMS molds were sterilized with 70% ethanol under UV irradiation for 1 hour, washed thrice with PBS and kept in the buffer at 37°C until use. PET Millicell Inserts (Millipore) with a 0.4 µm pore size were placed into wells and 300 µl of culture medium were added to each insert. Hydrogels were then washed twice with PBS to remove remaining ethanol and transferred to inserts. Negative controls (TCPS) consisted on inserts containing just complete medium; positive controls consisted on the use of complete medium supplemented with 1% phenol (Sigma-Aldrich) in both the wells and the inserts.

After a 42.5 hours incubation period at 37°C and 5% CO_2, cytotoxicity by indirect contact was assessed by cell quantification with Alamar blue and cell morphology examination. For cell shape visualization, cells were washed with Dulbecco´s phosphate-buffered saline (DPBS, Gibco), stained in the dark with 2 µM Calcein AM (Sigma-Aldrich) for 20 minutes at 37°C and washed with the buffer to remove excess dye. Images were acquired using an Eclipse TE200 inverted microscope (Nikon, Japan) and MetaMorph Microscopy Automation & Image Analysis Software (Molecular Devices, version 5.0r1).

2.5.2. Cell adhesion

Samples were prepared on 16-well Lab-Tek glass chamber slides (Nunc), stained with Trypan blue and washed until no apparent dye release was noticed. rMSCs were cultured as previously stated, seeded at a final density of $2.5 \cdot 10^3$ viable cells/sample and kept in complete medium for 24 hours. Samples were fixed with paraformaldehyde, permeabilized with 0.1% Triton X-100 (Sigma-Aldrich) for 5 minutes, blocked with PBS-gly supplemented with 6% bovine serum albumin (BSA; Sigma) for 45 minutes and stained in the dark at room temperature for vinculin and nuclei observation. Briefly, cell staining consisted on: (i) incubation with mouse anti-vinculin primary antibody (Sigma) at a 1/400 dilution in PBS-gly supplemented with 3% BSA (PBS-gly-BSA 3%) for 1h, (ii) incubation with Alexa 488-conjugated goat anti-mouse secondary antibody (Molecular Probes) at a 1/300 dilution in PBS-gly-BSA 3% for 1h, and (iii) incubation with 4 μg/ml 4',6-diamino-2-phenylindole dihydrochloride (DAPI, Sigma) for 2 minutes. Hydrogels were then mounted, sealed and observed by confocal microscopy. Volocity 3D Image Analysis Software (Perkin Elmer, version 6.2.1) was used to obtain 3D reconstructions.

2.6. Design of hydrogels with combined tailored properties

2.6.1. Surface stiffness

An EDC:COOH 9.3:1, COOH:NH_2 1.06:1 combination of molar ratios was selected to test the influence of polymer concentration on stiffness. Samples were prepared at 40, 54, 80 and 160 mg/ml polymer concentrations and stiffness was quantified as previously stated.

2.6.2. Structure of mechanically-tailored hydrogels

Hydrogels were prepared at a polymer concentration of 54 mg/ml using the EDC:COOH 9.3:1, COOH:NH_2 1.06:1 combination of molar ratios (from now on, RGD-C samples), incubated with 0.1 M Na_2HPO_4 for 3 h at RT and washed with PBS by performing swelling/shrinking cycles. Samples to be observed by confocal microscopy were stained with Trypan blue, and mounted

and visualized as previously stated. Hydrogels to be visualized by FESEM were subjected to serial dehydration in ethanol and critical point drying with CO_2. A voltage of 5 kV and a working distance of 6 mm were used to acquire images. The diameter of polymeric trabeculae was quantified using Fiji.

2.6.3. Cell proliferation on tailored hydrogels

Human MSCs (Lonza, Switzerland) were expanded in complete medium up to passage 8 ~~as previously stated~~. $2 \cdot 10^3$ cells/scaffold were seeded on RGD-C samples and on their 40 mg/ml, non-tailored counterparts. Seeded scaffolds were kept in culture for 1, 7, 14 and 21 days. For qualitatively assessing proliferation, samples were washed with PBS, cells were fixed with 3% paraformaldehyde as previously described, subjected to serial dehydration in ethanol and to critical point drying in CO_2. Hydrogels were then graphite-sputtered and visualized under a Quanta 200 Scanning Electron Microscope (SEM; FEI) at a 10 mm working distance and a 20 kV voltage.

For the quantitative assessment of cell proliferation in complete medium, hydrogels prepared in 96-well plates were degraded at days 1, 3, 7, 14 and 21 by using 2 mg/ml porcine pancreatic elastase in PBS for 3 h at 37ºC. After hydrogel degradation, M-PER (Thermos Scientific) was added to a 1:1 volume ratio and samples were subjected to three freezing/thawing cycles at -80ºC/RT. Cell lysates were transferred to microtubes and centrifuged at 2,500 g for 10 minutes at 4ºC using an Eppendorf 5415 R (Eppendorf, Germany) centrifuge. Cell debris were discarded and cleared cell lysates were used to quantify cell number by using the LDH-based Cytotoxicity detection kit plus (Roche) according to manufacturer's instructions. Briefly, cell lysates were incubated with reaction solution at a 1:1 volume ratio. Mixtures were incubated for 20 minutes at RT and absorbance was read at 490 nm using a reference wavelength of 600 nm.

2.6.4. Preliminary cell differentiation assays

For the assessment of alkaline phosphatase (ALP) expression, RGD-C hydrogels and their 40 mg/ml counterparts were prepared in 96-well plates and sterilized as previously stated. hMSCs were seeded at $2 \cdot 10^3$ cells/scaffold density and cultured in osteogenic medium (i.e. complete medium supplemented with 50 μg/ml ascorbic acid, 10 mM β-glycerolphosphate and 10 nM dexamethasone; osteogenic supplements from Sigma). At selected time points, scaffolds were degraded and cells were lysed as abovementioned. The expression of alkaline phosphatase (ALP) was quantified by using the SensoLyte pNPP alkaline phosphatase assay kit (AnaSpec). Briefly, cleared lysates were incubated with the p-Nytrophenyl phosphate (pNPP) substrate at a 1:1 volume ratio. Reagents were homogenized for few seconds and incubated at 37ºC for 40 minutes, and absorbance was read at 450 nm. ALP expression results were normalized to cell number.

For the assessment of osteopontin (OPN) expression, samples were prepared on 16-well Lab-Tek glass chamber slides, stained with Trypan blue, washed until no apparent dye release was noticed, and sterilized as previously mentioned. hMSCs up to passage 8 were seeded at $2 \cdot 10^3$ cells/scaffold density and cultured in osteogenic medium. At selected time points, cells were fixed, permeabilized and blocked as previously stated, and stained in the dark at room temperature for osteopontin (OPN) and nuclei visualization. Briefly, cell staining consisted on: (i) incubation with rabbit anti-OPN primary antibody (Abcam) at a 1/600 dilution in PBS-gly-BSA 3% for 1h, (ii) incubation with Alexa 488-conjugated goat anti-rabbit secondary antibody (Molecular Probes) at a 1/300 dilution in PBS-gly-BSA 3% for 1h, and (iii) incubation with DAPI for 2 minutes. Cells were then mounted with Mowiol 40-88, sealed and visualized by confocal microscopy.

2.6.5. *In vitro* mineralization

To assess citrate-related calcium phosphate nucleation capacity, citric acid-crosslinked hydrogels with tailored stiffness (RGD-C) were compared to samples crosslinked with glutaraldehyde (RGD-G).

RGD-G hydrogels were prepared at a polymer concentration of 54 mg/ml. Briefly, HRGD6 polymer was crosslinked with 5% glutaraldehyde (Sigma) for 7:30 h at 4ºC, reduced with 5% $NaBH_4$ (Aldrich) for 2 h on ice and washed with ultrapure water to remove remaining $NaBH_4$. RGD-C hydrogels were prepared as previously stated and washed several times with water to remove remaining reagents, by-products and salts. All samples were prepared in 6 mm-diameter PDMS molds. Simulated body fluids (SBF) were prepared as specified in the literature [17]. Samples were incubated with filtered, pre-warmed SBF at 37ºC for 1, 7, 14 and 28 days; SBF was replaced every 3 days. At endpoints, hydrogels were washed 3 times with ultrapure water and kept at 37ºC until the end of the experiment.

RGD-C samples were subjected to serial dehydration in ethanol and critical point drying with CO_2; RGD-G samples were frozen with liquid N_2 and lyophilized for two days. Hydrogels were then graphite-sputtered and analyzed using a Quanta 200 Scanning Electron Microscope equipped with a Genesis Energy Dispersive X-Ray Spectroscopy (EDS) system (EDAX, United States). A voltage of 20 kV and a working distance of 10 mm were used.

2.7. Statistical analysis

Data were analyzed by means of t-test or one-way ANOVA with Dunnett's post hoc test. All analyses were performed using Prism (GraphPad, version 6.01). Results were considered significant when $p \leq 0.05$ unless otherwise specified.

3. Results

3.1. Effect of reaction conditions on the crosslinking reaction

3.1.1 Gelation

Preliminary tests showed crosslinking was consistently achieved when reaction mixes prepared at 4ºC in MES buffer at an initial pH of ca. 6 were let to react for 1 hour at 37ºC (Data not shown). Under these conditions, hydrogels became gradually opaque during reticulation (Fig. 1a). This phenomenon made possible the monitoring of absorbance changes at a wavelength of 750 nm, at which none of the components showed remarkable light absorption. The increase in absorbance followed a sigmoidal curve that was mathematically derived to calculate latency time. This parameter was used to investigate how the relative abundance of reactive species (EDC and, -COOH and -NH_2 groups) involved in the reaction kinetically affect polymer aggregation. With this purpose, seven different hydrogels were prepared using particular combinations of EDC:COOH and COOH:NH_2 molar ratios (Fig. 1b). Latency time was found to be clearly influenced by the relative abundance of reactive species: increasing any of the two molar ratios led to a reduction in latency time (EDC:COOH, from 568.33±91.45 s to 371.11±6.97s; COOH:NH_2, from 371.11±6.97s to 120.77±26.37 s; Fig. 1c).

3.1.2. Quantification of unreacted –NH_2 groups

The number of primary amines remaining unreacted after reticulation was quantified by using TNBS [23]. Although HRGD6 polymer was designed to display ε-amino groups from lysine residues to be used for crosslinking purposes, α-amino groups from the N-terminus of polymeric chains may also participate in the EDC-mediated reaction. Thus, results presented herein correspond to the sum of unreacted α- and ε-amino groups.

As shown in figure 1d, increasing the EDC-to-COOH ratio did not have an effect on the percentage of primary amines involved in the reticulation reaction (all samples displayed ca.

46% free –NH_2), suggesting EDC is efficient even at a 2-fold molar excess respect to carboxyl groups for a fixed COOH:NH_2 ratio. In contrast, increasing the COOH:NH_2 ratio led to a remarkable decrease in the amount of unreacted amines, leading to an almost total consumption of –NH_2 groups in samples E9C5 (6.01±4.48% free –NH_2).

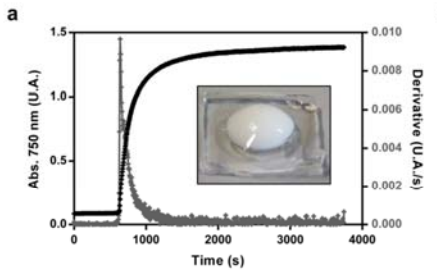

Sample code	EDC:COOH	COOH:NH_2
E2C1	1.88:1	1.06:1
E3C1	2.82:1	1.06:1
E5C1	4.7:1	1.06:1
E9C1	9.3:1	1.06:1
E9C2	9.3:1	2.16:1
E9C3	9.3:1	3.25:1
E9C5	9.3:1	5.44:1

Fig. 1. (a) Changes in absorbance ocurring during crosslinking reaction tracked at 750 nm (black) and mathematical derivative (gray), from which kinetic parameters were extracted. Inset: citric acid-crosslinked hydrogel at reaction completion; U.A. : Units of absorbance.(b) Detailed relative abundance of reactive species in reaction mixes used to prepare hydrogels. (c) Latency time calculated for all seven different samples. Plotting area was colored to clearly distinguish the separate contribution of the two molar ratios. (d)) Quantification of unreacted primary amines after crosslinking with citric acid and EDC. *p $value$≤0.05 with respect to E2C1 samples; **p $value$≤0.05 with respect to E9C1 samples.

3.2. Effect of reaction conditions on hydrogel properties

3.2.1. Hydrogels structure and polymer-occupied volume

The effect of molar ratios on hydrogel architecture was studied both by confocal microscopy and FESEM. Observation of the structure by confocal microscopy was possible due to hydrogels'

inner autofluorescence, which was red-shifted and intensified by staining with Trypan blue (Data not shown). This phenomenon allowed the visualization of three different architectures (globular, globulo-fibrillar and dense) and structural changes regarding polymer aggregation, aggregate size and matrix density. Polymer in E2C1 samples assembled in the form of globules with a diameter of ca. 3 μm (Fig. 2a). Increasing EDC:COOH to obtain E3C1 samples led to a transitional structure in which large aggregates and nascent elongated entities (trabeculae) formed by smaller aggregates (diameter of ca. 1.5 μm) were observed (Fig. 2b). E5C1 and E9C1 samples displayed architectures enriched with fiber-like structures where polymer aggregates had a diameter of ca. 1.3 μm and 1.2 μm, respectively (Fig. 2c and d). Although it was not possible measuring the size of aggregates in E9C2, E9C3 and E9C5 samples, increasing COOH:NH_2 seemingly led to a reduction of the aggregate and trabeculae size down to the nanoscale (fig. 2f-h). This latter phenomenon was accompanied by an increase in hydrogels density.

FESEM was used to confirm what was observed by confocal microscopy. No globules were observed in any of the samples. However, changes in the density of the structure and in polymer aggregation were confirmed. Increasing EDC:COOH molar ratio led to mesh constituents transitioning from irregular-shaped (Fig. 2a2) to thin connecting fiber-like entities or trabeculae (Fig. 2b2-d2). Increasing the COOH-to-NH_2 ratio led to obtaining hydrogels with dense structures displaying sublimation-derived pores typical of lyophilized hydrogels[24] (Fig. 2f2-h2).

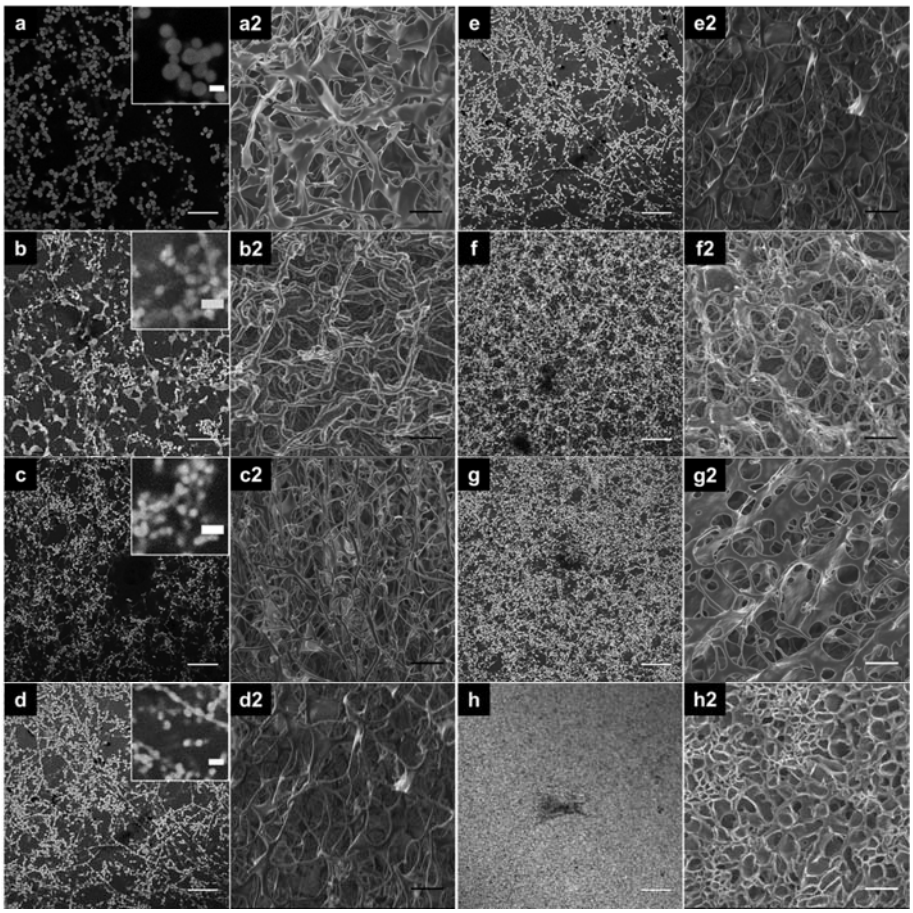

Fig. 2. The architecture of hydrogels prepared using specific combinations of molar ratios visualized under confocal microscopy (a-h) and FESEM (a2-h2). Images a-h are representative confocal microscopy slices displaying the characteristic architecture of citric acid-crosslinked hydrogels prepared in different reaction conditions. a,a2: E2C1; b, b2: E3C1; c, c2: E5C1; d-e, d2-e2: E9C1; f, f2: E9C2; g, g2: E9C3; h, h2: E9C5. Insets in images a-d illustrate changes in the size of polymer aggregates induced by using increasing COOH:NH_2 molar ratios while keeping the EDC-to-COOH ratio constant. Confocal microscopy scale bar: 20 μm; inset scale bar: 3 μm. FESEM scale bar: 5 μm.

In order to confirm the apparent effect of excess –COOH with respect to –NH_2 on scaffold density, sections obtained by confocal microscopy were processed to quantify the volume occupied by HRGD6 polymer (3D reconstructions of calculated volumes compared to the

original 3D sections can be seen in Fig. S1). The EDC:COOH ratio was found not to affect PV/TV; in contrast, COOH:NH_2 had a strong effect on reducing the void volume (from 31.56±0.69% to 74.09±7.33% of polymer-occupied volume; Fig. 3a) in such a way that the higher the COOH-to-NH_2 ratio, the more dense the scaffold.

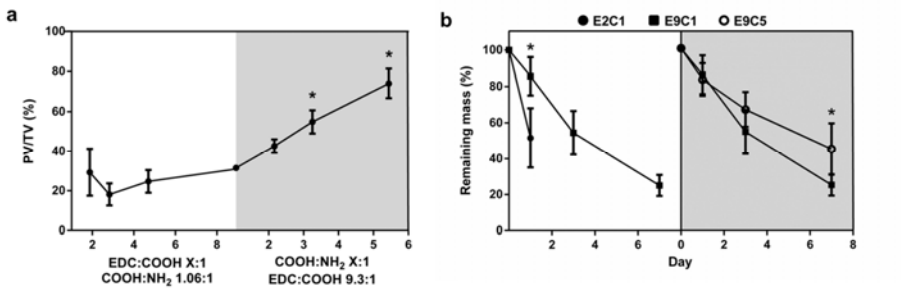

Fig. 3. (a) Quantification of the percentage of polymer-occupied volume (PV/TV) in hydrogels prepared under different conditions. (b) Degradation profiles of selected hydrogels after *in vitro* exposure to porcine pancreatic elastase; (left) E2C1 and E9C1 samples; (right) E9C1 and E9C5 samples. **p value*≤0.01.

3.2.2. Resistance to enzymatic degradation

To investigate differences between samples regarding resistance to enzymatic degradation, hydrogels were incubated with porcine pancreatic elastase. In order to simplify the experiments and to provide a proof of concept, 3 out of the 7 different hydrogels were chosen to be used in this part of the study: E2C1, E9C1 and E9C5. E2C1 samples were found to degrade quickly, losing ca. 50% of their mass within the first day and being completely dissolved by day 3 (Fig. 3b, left). In contrast, E9C1 hydrogels showed reduced degradation at day 1 and sustained mass loss along the experiment, by the end of which ca. 75% of the material had been digested. E9C5 samples showed a significantly reduced mass loss rate from day 3 to day 7, at which ca. 55% of the material had been enzymatically processed (Fig. 3b, right).

3.2.3. Surface stiffness

An interesting question to answer was whether the apparent differences regarding crosslinking yield and structure between samples would influence their mechanical properties at a surface level. As it is shown in table 1, stiffness was seemingly unaffected by molar ratios, none of which proved useful to mechanically tailor citric acid-crosslinked hydrogels. Additionally, none of the samples was shown to possess a Young's modulus value in the range of interest (25-40 kPa [4]).

Sample code	Young's modulus (kPa)
E2C1	1.81 ± 1.56
E3C1	10.37 ± 6.53
E5C1	3.32 ± 1.87
E9C1	7.85 ± 5.51
E9C2	3.13 ± 1.75
E9C3	7.26 ± 3.26
E9C5	5.19 ± 4.46

Table 1. Young's modulus of citric acid-crosslinked hydrogels prepared at a 40 mg/ml polymer concentration.

3.3. Effect of reaction conditions on hydrogels cytotoxicity and RGD integrity

3.3.1. Cytotoxicity

Indirect contact experiments were performed to test hydrogels for the release of excess EDC and its toxic by-product, N-acylurea. Again, E2C1, E9C1 and E9C5 samples were selected to simplify the experiment. Cells were seeded on tissue culture polystyrene (TCPS), let to adhere for 4 hours and quantified. Results were normalized to cell number in the negative control. No differences in cell number were observed (Fig. 4a), assuring all wells used in the experiment had approximately the same initial cell density, thus avoiding artifacts due to uneven adhesion. Cells were exposed to different agents for 42.5 h and quantified again. After normalization, it was

found E2C1 and E9C1 samples led to an increased number of cells when compared to that in TCPS. In contrast, E9C5 hydrogels produced a decrease in cell number of about 70%. No cell survival was observed in those wells treated with culture medium supplemented with 1% phenol. After staining with Calcein AM, cells exposed to culture medium and samples E2C1 and E9C1 were found to display normal morphology (Fig. 4b); exposure to E9C5 induced morphological alterations. No cells were observed in those wells treated with 1% phenol (Data not shown).

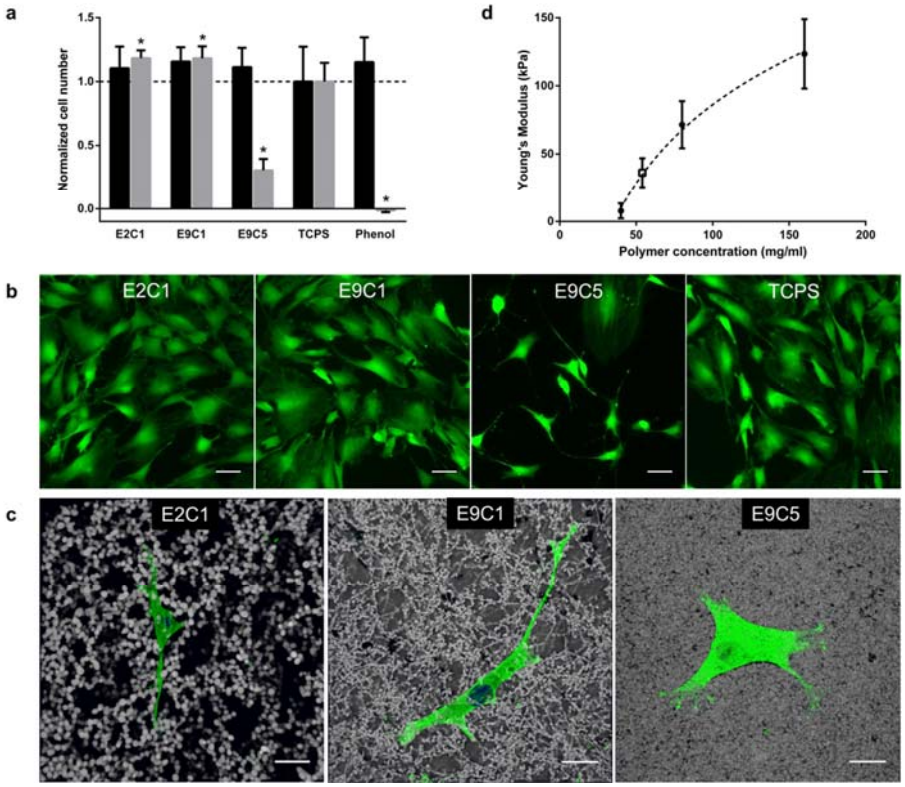

Fig. 4. (a) Citotoxicity assessment of selected hydrogels by indirect contact. Cell numbers were quantified after adhesion (black bars) and after a 2-days exposure period (gray bars), and normalized to those in the control surface (TCPS) for each time point. (b) Morphology of rMSCs exposed to hydrogels and to control surface for 2 days; scale bar: 20 μm. (c) rMSCs on selected samples after preliminary 24-hour cultures. Green: vinculin; blue: nuclei. Scale

bar: 20 μm. (d) Effect of polymer concentration on stiffness (filled dots) and Young's modulus of E9C1 samples prepared at a 54 mg/ml polymer concentration (empty square). *p *value*≤0.001 with respect to TCPS.

3.3.2. Cell adhesion

Cell adhesion experiments were performed to test hydrogels for RGD integrity. rMSCs were seeded on the surface of hydrogels and kept in culture for 24 hours. Immunocytochemical staining revealed cells adhered to hydrogels regardless of their architecture (Fig. 4c) and produced filopodia able to penetrate those matrices with an open structure (Fig. S2). Cells displayed normal morphology in all cases, although focal contacts were just observed in those samples with a dense matrix structure, in which nuclei were not visualized due to the strong autofluorescence of E9C5 samples in the $\lambda_{emission}$= 430-476 nm range.

3.4. Design of hydrogels with combined tailored properties

3.4.1. Surface stiffness

Given molar ratios were found not useful to achieve target Young's modulus, the effect of a third variable, polymer concentration, was explored. The E9C1 setup was chosen to study how polymer concentration influences stiffness at a surface level. The use of different amounts of polymer led to obtaining a logarithmic function from which the polymer concentration needed to achieve hydrogels with target Young's modulus was extrapolated (Fig. 4d). A Young's modulus in the 25-40 kPa range is considered to be osteogenic; a modulus of 34 kPa was specifically targeted given that it has been already shown to induce the expression of osteogenic markers [4]. E9C1 hydrogels with a polymer concentration of 54 mg/ml -corresponding to a theoretical stiffness of 34.83 kPa- exhibited an experimental value of 36.13±10.72 kPa.

3.4.2. Structure of mechanically-tailored hydrogels

Mechanically-tailored RGD-C hydrogels (i.e. E9C1 samples prepared at a polymer concentration of 54 mg/ml) were analyzed by confocal microscopy and FESEM. Sections obtained by confocal

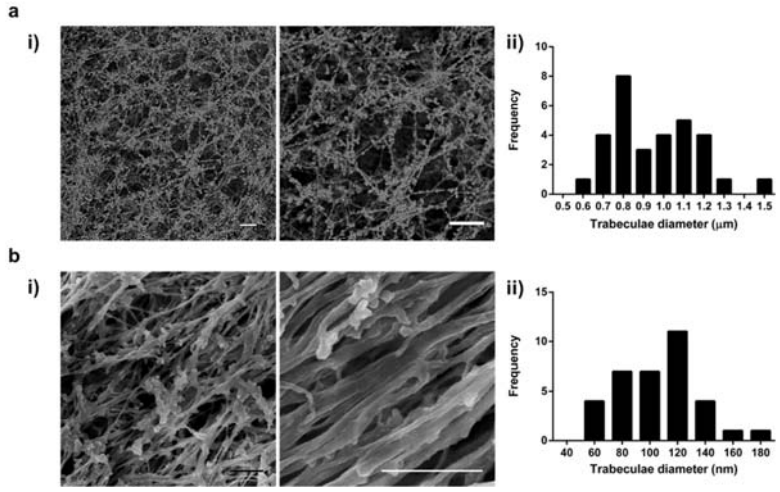

Fig. 5. Study of the structure of 54 mg/ml hydrogels under (a) confocal microscopy and (b) FESEM. i) Detailed visualization and ii) size distribution of fiber-like entities in hydrogels with tailored stiffness. Confocal microscopy scale bar: 20 μm; FESEM scale bar: 1 μm.

microscopy revealed RGD-C samples retained the fiber-like architecture seen in their 40 mg/ml counterparts (Fig. 5a, i). Polymer globules in RGD-C hydrogels organized in the form of fiber-like entities (trabeculae) with a diameter of 952.64 ± 210.57 nm (Fig. 5a, ii). Under FESEM, RGD-C samples were found to possess a reduced number of globules and to be shaped by trabeculae with a diameter of 106.30 ± 30.75 nm that locally arranged with varying degrees of alignment (Fig. 5b, i and ii).

3.4.3. Cell proliferation on tailored hydrogels

The proliferation of hMSCs on RGD-C hydrogels and on their 40 mg/ml counterparts was qualitatively and quantitatively assessed. Cells were found to adhere and spread, displaying a normal morphology in both types of samples at all time points (Fig. 6a). Cell numbers in hydrogels were significantly higher than those in TCPS (Fig. 6b) at days 3 (4269.3 ± 697.8 in 54 mg/ml samples, 3610.7 ± 460 in 40 mg/ml samples, and 289.3 ± 267.3 in TCPS), 7 (10633.3 ±

1037.3 in 54 mg/ml matrices, 10062.7 ± 575.1 in 40 mg/ml samples, and 458.7 ± 148 in TCPS) and 14 (29636.7 ± 7706.3 in 54 mg/ml hydrogels, 34040 ± 9127.5 in 40 mg/ml hydrogels, and 11286.7 ± 993.2 in TCPS); by the end of the experiment, just RGD-C samples displayed cell numbers significantly higher than those in TCPS (71206.7 ± 25666.2 in 54 mg/ml hydrogels, 51953 ± 4437.7 in 40 mg/ml hydrogels, and 29120 ± 13286.96 in TCPS). No statistically significant differences between hydrogels were noticed at any time point.

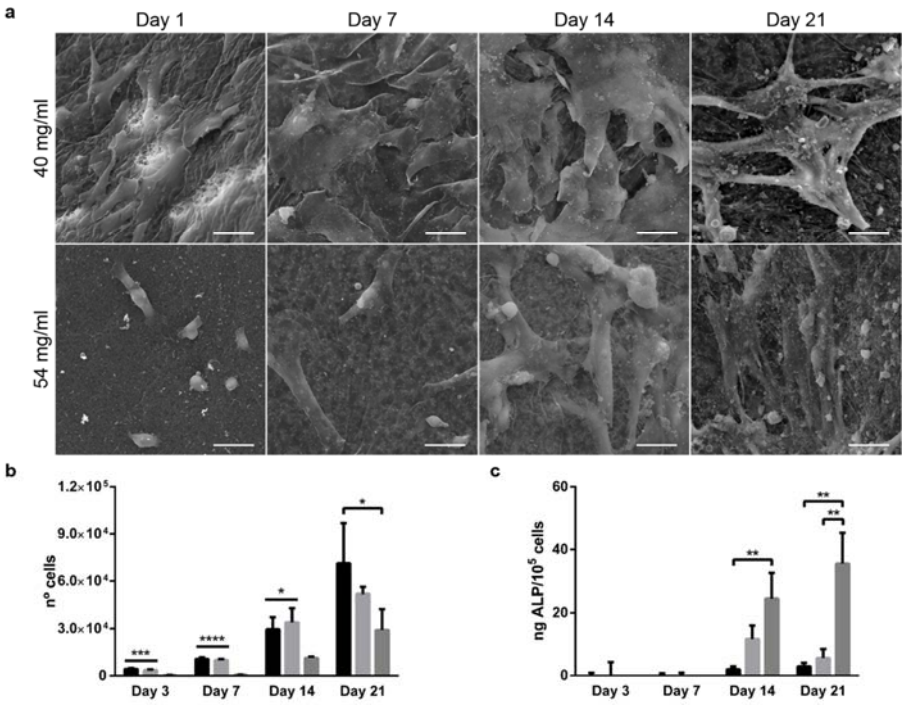

Fig. 6. (a) Qualitative and (b) quantitative assessments of proliferation, and (c) ALP expression of hMSCs seeded on 40 mg/ml and 54 mg/ml hydrogels. Scale bar: 50 μm. Black bars: 54 mg/ml; light grey bars: 40 mg/ml; dark grey bars: TCPS. *p value≤0.05; **p value≤0.01, ***p value≤0.001, ****p value≤0.0001.

3.4.4. Preliminary cell differentiation assays

The osteogenic differentiation of hMSCs on hydrogels was tested by assessing the expression of ALP and OPN. Cells were found to display a late expression of ALP, as evidenced by ALP first appearing at day 14 (Fig. 6c). Overall, cells cultured in TCPS were found to express higher levels of the marker both at days 14 (1.94 ± 0.92 ng/10^5 cells in 54 mg/ml samples, 11.69 ± 4.24 ng/10^5 cells in 40 mg/ml samples, and 25.54 ± 8 ng/10^5 cells in TCPS) and 21 (2.85 ± 1.17 ng/10^5 cells in 54 mg/ml hydrogels, 5.58 ± 2.86 ng/10^5 cells in 40 mg/ml hydrogels, and 35.46 ± 9.89 ng/10^5 cells in TCPS). Despite cells cultured in 40 mg/ml matrices expressed ALP levels higher than those cultured in RGD-C samples, no statistically significant differences were noticed between hydrogels.

Additionally, the expression of OPN was assessed by immunofluorescence. As shown in figure 7, cells cultured on TCPS and on hydrogels displayed an OPN expression increasing along the experiment. Overall, cells cultured on hydrogels expressed lower amounts of OPN in comparison to those cultured on TCPS. Interestingly, cells in mechanically-tailored hydrogels seemingly expressed higher amounts of OPN than those in non-tailored counterparts both at days 14 and 21.

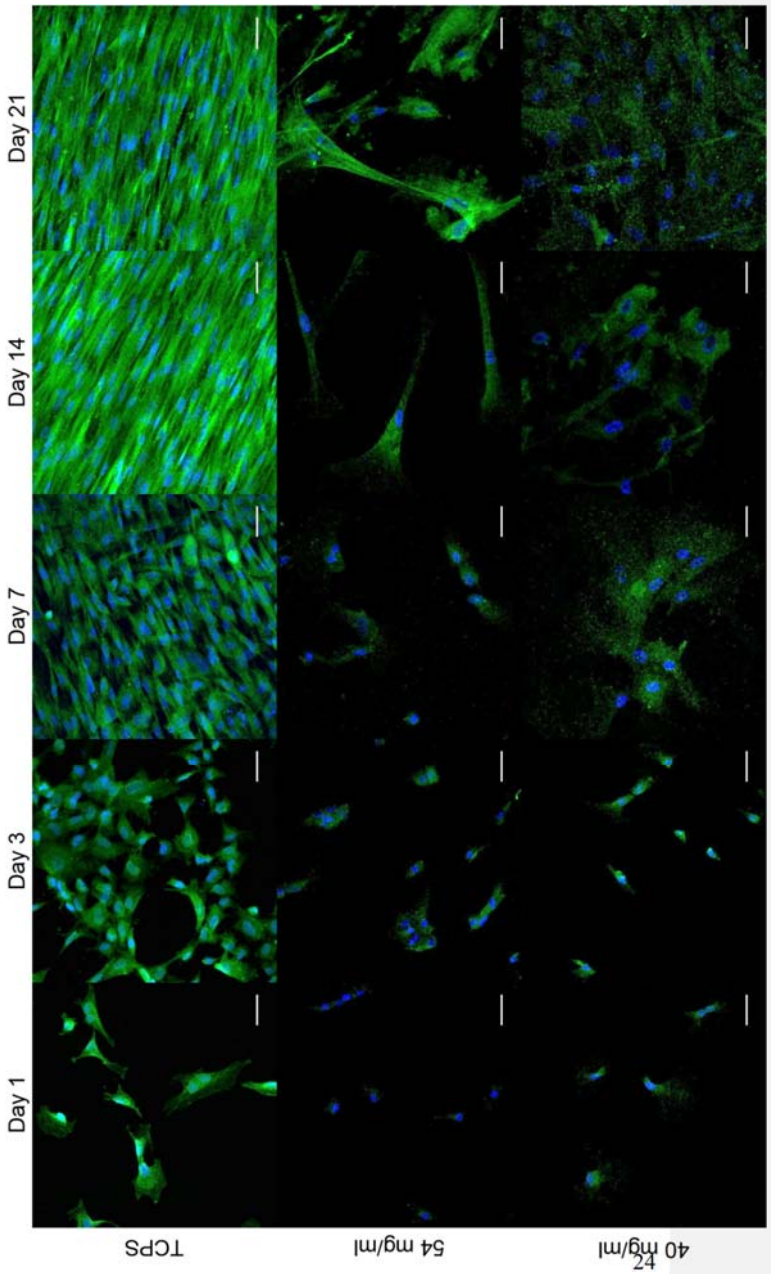

Fig. 7. Expression of osteopontin in hMSCs cultured on TCPS and on hydrogels. Scale bar: 50 µm.

3.4.4. *In vitro* mineralization

RGD-C hydrogels were tested for citric acid-related mineralization capacity using SBF 1x. RGD-G samples were included in this experiment in order to account for HRGD6-derived nucleation capacity, if any. No calcium phosphates were found on glutaraldehyde-crosslinked hydrogels at any time point (Data not shown). In contrast, sparse mineral deposits with a Ca/P ratio of ca.

1.8 were detected in RGD-C hydrogels at all time points (Fig. 8).

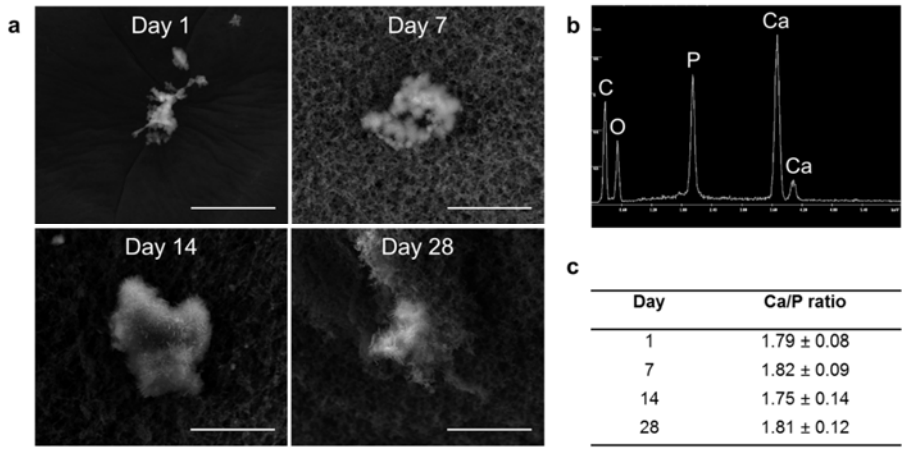

c

Day	Ca/P ratio
1	1.79 ± 0.08
7	1.82 ± 0.09
14	1.75 ± 0.14
28	1.81 ± 0.12

Fig. 8. *In vitro* mineralization of RGD-C hydrogels by using SBF 1x. (a) Detail on the sparse mineral deposits found along the experiment. Scale bar: 20 μm. (b) Representative EDS profile showing the presence of calcium phosphates. (c) Calcium/phosphate ratio of mineral deposits found at different time points.

4. Discussion

The present study aimed to design biomimetic hydrogels for *in situ* bone tissue engineering. HRGD6 elastin-like recombinamer was crosslinked with citric acid by means of EDC-mediated catalysis. EDC and citric acid have already been combined to produce hydrogels involving the multistep, time-consuming chemical synthesis of N-hydroxysuccinimide esters of citric acid that can be then used to crosslink polymers containing free primary amines [25]. In the present study, citric acid-crosslinked hydrogels were produced through a one-step, organic solvent-free reaction performed in mild conditions.

Carbodiimide-mediated activation of carboxylic acids (-COOH) to achieve the formation of peptide bonds is known to be affected by different parameters such as pH [13,26], reaction time [26,27], and EDC:COOH [26] and COOH:NH_2 [27] molar ratios. After previous optimization, seven setups characterized by particular combinations of EDC:COOH and COOH:NH_2 molar

ratios were prepared (Fig. 1b) at 4ºC and pH≈6, and let to react for 1 h at 37ºC. Under these conditions, the reticulation reaction was characterized by an increase in turbidity following a sigmoidal curve (Fig. 1a), a phenomenon already described for decellularized extracellular matrix [28] and a variety of polysaccharides and proteins such as coagulin [29], fibrin [30] and agarose [31]. A typical analysis of this phenomenon involves dividing the reticulation curve into three main stages: (i) lag phase or induction period (herein, latency time), (ii) network growth stage and (iii) pseudo-equilibrium stage [31].

HRGD6 polymer has the ability to self-aggregate in response to changes in temperature and pH, displaying an inverse transition temperature [32] (ITT) of 32ºC in PBS at pH=7.4, although ITT would be somewhat lower at the pH used herein [20]. During latency time, the temperature of the solution gradually rises along the incubation period. When the solution reaches the ITT, polymer molecules undergo conformational rearrangement leading to intermolecular hydrophobic aggregation [33], giving rise to supramolecular aggregates with size increasing up to few micrometers over time [34]. In the presence of a crosslinker, aggregates are linked to each other, thus conferring hydrogels their characteristic nano-microarchitecture (network growth and pseudo-equilibrium stages). On this basis, it was hypothesized that the length of latency time, found to be affected by both molar ratios (Fig. 1c), would have a direct effect on the size of polymer aggregates building up citric acid-crosslinked hydrogels, in such a way that the shorter the latency time, the smaller the aggregates shaping the network.

The amount of $–NH_2$ groups remaining unreacted after crosslinking was quantified for all seven hydrogels and found to be remarkably affected by the COOH-to-NH_2 molar excess (Fig. 1d). Specifically, the higher the COOH:NH_2 molar ratio, the higher the amount of $–NH_2$ groups involved in the reaction, boosting the number of crosslinking points and thus reducing polymer

chain mobility and inter-chain void space[35]. As shown in figures 1d and 3a, the polymer-occupied volume (i.e. hydrogel density) increases as the number of unreacted groups diminishes, suggesting the degree of crosslinking, along with latency time, define the architecture of citric acid-crosslinked hydrogels.

The structure of scaffolds prepared using different reaction conditions was studied (Fig. 2). As revealed by confocal microscopy, the EDC:COOH molar ratio affects (i) polymer aggregation, which ranged from purely globular to globulo-fibrillar (i.e. globules organized in the form of fibrous structures), and (ii) aggregate size, which is also seemingly affected by the COOH-to-NH_2 molar excess. Additionally, the COOH:NH_2 ratio influences hydrogel density (as confirmed by FESEM observations and PV/TV calculations), an increase in which is likely to be the consequence of reduced aggregate size and of increased globule interconnectivity. Together, these results support the hypotheses that latency time and crosslinking degree dictate the organization of HRGD6 polymer thus defining the architecture of herein described hydrogels. Furthermore, they point out the architecture of citric-acid crosslinked hydrogels can be tuned by using specific combinations of EDC:COOH and COOH:NH_2 molar ratios.

FESEM failed to reveal the nano-microstructure (globules) seen by confocal microscopy, which was presumably lost during sample preparation for their visualization under electron microscopy (Fig. 2 and 5). This phenomenon proved the usefulness of red-shifting samples' autofluorescence with trypan blue to visualize hydrogels' intact structural features when no nanometric resolution is required. This is a cheap, fast and easy method to visualize hydrogel architecture, to perform structural calculations such as PV/TV or to visualize how cells interact with scaffolds (Fig. S2) in short duration cultures without the need of going through fluorophore grafting protocols.

The resistance to *in vitro* degradation of selected samples (E2C1, E9C1 and E9C5) was assessed. The amount of unreacted $–NH_2$ groups and PV/TV for E2C1 and E9C1 samples are not significantly different (Figures 1d and 3a). However, E9C1 hydrogels showed improved resistance to enzymatic degradation (Fig. 3b, left). Structurally, when increasing EDC:COOH, there was an apparent reduction in the occurrence of dangling polymeric ends accompanied by an increase of trabeculae interconnectivity (Fig. 2a2-d2), which would be the reason for the increased stability of E9C1 hydrogels compared to that of E2C1 ones. E9C5 samples displayed improved resistance to degradation in comparison to E9C1 gels (Fig. 3b, right), which would be due to (i) a higher polymer network connectivity [36] derived from a much higher consumption of $–NH_2$ groups[37] (Fig. 1d), and (ii) a consequently increased PV/TV (Fig. 3a) further limiting enzyme accessibility and ultimately slowing down degradation. Given network and structural features are dependent on the reaction conditions used to prepare structurally tailored scaffolds, it is noteworthy that the degradation of citric acid-crosslinked HRGD6 hydrogels cannot be independently tuned.

Hydrogels were tested for cytocompatibility by indirect contact with rMSCs. E2C1, E9C1 and E9C5 samples were selected to simplify indirect cytotoxicity assays. After a 42.5 hour-exposure period, cell number in wells exposed to E2C1 and E9C1 samples was significantly higher than that in control wells (Fig. 4a). This phenomenon could be due to the release of unbound or partially bound citric acid, which would be incorporated into the cell through the Na-coupled citrate transporter; once in the cytosol, citrate would be turned into lipids to meet the requirements for MSCs proliferation-related membranogenesis [38]. In contrast, E9C5 samples led to a highly reduced viability and altered cell morphology (Fig. 4b), most likely due to the slow release of N-acylurea, the toxic and water-soluble by-product of EDC. This would be due to

an incomplete removal of N-acylurea during the washing steps because of reduced diffusion in dense E9C5 hydrogels, leading to the slow release of the by-product during the experiment. This cytotoxic effect was not noticed when rMSCs were seeded on E9C5 hydrogels (Fig. 4c), most likely due to the extra washes applied after pre-staining with trypan blue. Cell adhesion experiments revealed that rMSCs were able to adhere to all seven hydrogels, suggesting –COOH groups from aspartic acid's side chain are not involved in the EDC-mediated reaction in the conditions used herein, so RGD tripeptides remain unaffected and functional for cells to attach to them.

The effect of the relative reactive species abundance on hydrogels mechanical properties was studied. Given molar ratios were found not useful to tune stiffness (Table 1), the influence of polymer concentration was explored. To do so, the E9C1 setup was chosen since it led to obtaining cytocompatible hydrogels possessing fiber-like microstructure and ca. 45% of free primary amines, a functional group shown to induce and maintain the osteogenic differentiation of MSCs [5,39]. After preparing E9C1 hydrogels at different polymer concentrations, 54 mg/ml was extrapolated (Fib. 4d) as the concentration needed to achieve samples with a target Young's modulus value of 34.83 kPa. Experimentally, RGD-C hydrogels were shown to possess a Young's modulus of 36.13±10.72 kPa and to retain its 40mg/ml counterpart's fiber-like structure (Fig. 5a). Interestingly, these results point out that the structure and surface stiffness of citric acid-crosslinked hydrogels can be separately tuned by modifying the combination of molar ratios and the polymer concentration used to prepare them, respectively.

Proliferation assays showed that both mechanically-tailored and non-tailored hydrogels supported the adhesion, spreading and proliferation of hMSCs (Fig. 6a and b), once again evidencing that the integrity of RGD tripeptides is preserved during EDC-catalyzed crosslinking

with citric acid. Overall, hydrogels led to significantly increased cell numbers suggesting that they provide at least a 2.5D environment for cell (in)growth.

Differentiation assays revealed a reduced and seemingly delayed expression of ALP (Fig. 6c) and OPN (Fig. 7) in cells cultured on hydrogels in comparison to that in cells seeded on TCPS, suggesting that most of the cells in hydrogels were in a proliferative state while some of them would have activated the differentiation machinery. No statistically significant differences between hydrogels were observed as to the expression of ALP; despite an apparent low cell number presumably due to the release of trypan blue (Fig. 7), OPN expression at days 14 and 21 in cells cultured on RGD-C hydrogels was seemingly higher than in those cultured on their non-mechanically tailored counterparts. Despite OPN expression results suggest that RGD-C matrices may represent an advantage as to the induction of osteogenic differentiation, longer cultures would be required to detect clear differences between hydrogels as to their osteogenic potential.

RGD-C hydrogels were also shown to nucleate calcium phosphate when incubated with SBF 1x. Although sparse at all time points, mineral deposits were found even by day 1 and kept a quite stable Ca/P ratio along the experiment (Fig. 8). The presence of mineral phase in RGD-C but not in RGD-G hydrogels points out unreacted –COOH groups from citric acid provide HRGD6 polymer with apatite-nucleating capacity [40], suggesting RGD-C hydrogels would be able to bond to damaged bone. Additionally, the early formation of apatite *in vitro* suggests that hydrogel-to-bone bonding would occur shortly upon implantation [17], helping the scaffold to stay in place and thus reducing the risk of incomplete defect closure due to scaffold misplacement.

The production of hydrogels for bone regeneration exhibiting calcium phosphate-nucleation capacity has gained momentum in the last years due to hydroxyapatite's osteogenic potential [18,19]. Mineralizing hydrogels can be achieved by means of strategies such as the post-gelation partial hydrolysis to expose –COOH groups [41], functionalization with carboxylate-terminated spacers [42], or the use of polymers, either recombinantly [10,43] or chemically-synthetized [44], containing hydroxyapatite-binding motifs. Post-gelation treatments and functionalization usually require the use of chemicals that can compromise the biocompatibility of the construct, while those hydrogels with internal nucleation motifs possess a polymer-dependent mineralization capacity. In contrast, our hydrogels are produced in mild conditions and display citric acid-dependent mineralization capacity. Citric acid, used herein both as a non-toxic crosslinker and a calcium phosphate-nucleating molecule, possesses carboxylates spaced by a distance matching that spacing calcium ions in hydroxyapatite and thus has been suggested to be both a natural HA-stabilizing and nucleating molecule [15]. Interestingly, it can be used in combination with EDC to produce hydrogels as long as the polymer to be crosslinked contains enough $–NH_2$ groups, making this method a versatile strategy to achieve mineralizing hydrogels for bone regeneration.

~~*In vitro and*~~ *in vivo* biological experiments are currently ongoing to disclose the osteoconductive potential of RGD-C hydrogels.

5. Conclusions

Elastin-like recombinamers were crosslinked with citric acid through an organic solvent-free, and time and cost-effective reaction. The effect of crosslinking conditions on hydrogel properties such as structure, stiffness, degradation and cytotoxicity was assessed. This systematic study allowed gaining control of the reticulation process to independently tune architecture and

mechanical properties to obtain microstructured hydrogels with intact cell adhesion motifs, fiber-like architecture, biomimetic Young's modulus and mineralization capacity, with the latter being attributable to citric acid. To our knowledge, this is the first time citric acid is used both as a crosslinker and a bioactive molecule providing hydrogels aiming bone regeneration with calcium phosphate nucleation capacity. Interestingly, the established protocol can be potentially applied to natural polypeptides exposing $-NH_2$ groups, such as collagen I, to produce self-mineralizing scaffolds with a superior degree of biomimetism.

Additionally, a method to study "near-*in vitro*" hydrogel structural features and visualize cell-material interactions at the microscale has been developed. This method may bypass the need of performing SEM when resolution in the nanoscale is not required and is believed to be of great usefulness during the development of hydrogels based on valuable natural or nature-inspired polymers.

Herein developed mechanically-tailored and microstructured hydrogels supported the growth of hMSCs and apparently represent an advantage regarding osteogenic differentiation when compared to non-tailored counterparts, as revealed by preliminary OPN expression assays. Further differentiations experiments are required to confirm this results.

Acknowledgements

Authors want to thank Dr. Adam Engler, Dr. Alexander Fuhrmann and Matthew Ondeck for his assistance with Young's modulus measurements and calculations; Dr. Elena Rebollo, from the Advanced Fluorescence Microscopy unit at the Molecular Biology Institute of Barcelona (IBMB-CSIC), for her unmatched technical training and guidance on confocal microscopy and for valuable discussion; and Judit Linacero, from The Nanotechnology Platform at IBEC, for her technical assistance with FESEM. Funding was provided by the European Union (projects

Comentado [EE1]: Falta la filiació

NMP3-LA-2011-263363, HEALTH-F4-2011-278557 and MSCA-ITN-2014-ETN-642687), the Spanish Ministry of Science and Innovation (MICINN; projects MAT2009-14195-C03-02, MAT2012-38043-C02-01, MAT2013-41723-R and MAT2013-42473-R) and the local government of Castillae-Leon (projects VA244U13 and VA313U14).

References

[1] Behonick DJ, Werb Z. A bit of give and take: the relationship between the extracellular matrix and the developing chondrocyte. Mech Dev 2009;120:1327–36.

[2] Schwartz MA, Schaller MD, Ginsberg MH. Integrins: emerging paradigms of signal transduction. Annu Rev Cell Dev Biol 1995;11:549–99.

[3] Oh S, Brammer KS, Li YSJ, Teng D, Engler AJ, Chien S, et al. Stem cell fate dictated solely by altered nanotube dimension. Proc Natl Acad Sci U S A 2009;106:2130–5.

[4] Engler AJ, Sen S, Sweeney HL, Discher DE. Matrix elasticity directs stem cell lineage specification. Cell 2006;126:677–89.

[5] Curran JM, Chen R, Hunt JA. The guidance of human mesenchymal stem cell differentiation in vitro by controlled modifications to the cell substrate. Biomaterials 2006;27:4783–93.

[6] Reyes CD, García AJ. Alpha2beta1 integrin-specific collagen-mimetic surfaces supporting osteoblastic differentiation. J Biomed Mater Res A 2004;69:591–600.

[7] Rowlands AS, George PA, Cooper-White JJ. Directing osteogenic and myogenic differentiation of MSCs: interplay of stiffness and adhesive ligand presentation. Am J Physiol Cell Physiol 2008;295:C1037–44.

[8] Lee J, Abdeen AA, Zhang D, Kilian KA. Directing stem cell fate on hydrogel substrates by controlling cell geometry, matrix mechanics and adhesion ligand composition. Biomaterials 2013;34:8140–8.

[9] Welsh ER, Tirrell DA. Engineering the extracellular matrix: A novel approach to polymeric biomaterials. I. Control of the physical properties of artificial protein matrices designed to support adhesion of vascular endothelial cells. Biomacromolecules 2000;1:23–30.

[10] Prieto S, Shkilnyy A, Rumplasch C, Ribeiro A, Arias FJ, Rodríguez-Cabello JC, et al. Biomimetic calcium phosphate mineralization with multifunctional elastin-like recombinamers. Biomacromolecules 2011;12:1480–6.

[11] Girotti A, Reguera J, Rodriguez-Cabello JC, Arias FJ, Alonso M, Testera AM. Design and bioproduction of a recombinant multi(bio)functional elastin-like protein polymer containing cell adhesion sequences for tissue engineering purposes. J Mater Sci Med 2004;15:479–84.

[12] Lee F, Chung JE, Kurisawa M. An injectable enzymatically crosslinked hyaluronic acid–tyramine hydrogel system with independent tuning of mechanical strength and gelation rate. Soft Matter 2008;4:880.

[13] Nakajima N, Ikada Y. Mechanism of amide formation by carbodiimide for bioconjugation in aqueous-media. Bioconjug Chem 1995;6:123–30.

[14] Hartles RL. Citrate in mineralized tissues 1964:225–53.

[15] Hu Y-Y, Rawal A, Schmidt-Rohr K. Strongly bound citrate stabilizes the apatite nanocrystals in bone. Proc Natl Acad Sci U S A 2010;107:22425–9.

[16] Rhee SH, Tanaka J. Effect of citric acid on the nucleation of hydroxyapatite in a simulated body fluid. Biomaterials 1999;20:2155–60.

[17] Kokubo T, Takadama H. How useful is SBF in predicting in vivo bone bioactivity? Biomaterials 2006;27:2907–15.

[18] Phadke A, Shih Y-R V, Varghese S. Mineralized synthetic matrices as an instructive microenvironment for osteogenic differentiation of human mesenchymal stem cells. Macromol Biosci 2012;12:1022–32.

[19] Kim SE, Choi HW, Lee HJ, Chang JH, Choi J, Kim KJ, et al. Designing a highly bioactive 3D bone-regenerative scaffold by surface immobilization of nano-hydroxyapatite. J Mater Chem 2008;18:4994.

[20] Costa RR, Custódio CA, Testera AM, Arias FJ, Rodríguez-Cabello JC, Alves NM, et al. Stimuli-responsive thin coatings using elastin-like polymers for biomedical applications. Adv Funct Mater 2009;19:3210–8.

[21] Schindelin J, Arganda-Carreras I, Frise E, Kaynig V, Longair M, Pietzsch T, et al. Fiji: an open-source platform for biological-image analysis. Nat Methods 2012;9:676–82.

[22] Doube M, Kłosowski MM, Arganda-Carreras I, Cordelières FP, Dougherty RP, Jackson JS, et al. BoneJ: free and extensible bone image analysis in ImageJ. Bone 2010;47:1076–9.

[23] Bubnis WA, Ofner CM. The determination of epsilon-amino groups in soluble and poorly soluble proteinaceous materials by a spectrophotometric method using trinitrobenzenesulfonic acid. Anal Biochem 1992;207:129–33.

[24] Kang HW, Tabata Y, Ikada Y. Fabrication of porous gelatin scaffolds for tissue engineering. Biomaterials 1999;20:1339–44.

[25] Saito H, Taguchi T, Kobayashi H, Kataoka K, Tanaka J, Murabayashi S, et al. Physicochemical properties of gelatin gels prepared using citric acid derivative. Mater Sci Eng C-Biomimetic Supramol Syst 2004;24:781–5.

[26] Olde Damink LHH, Dijkstra PJJ, van Luyn MJA, van Wachem PB, Nieuwenhuis P, Feijen J, et al. Cross-linking of dermal sheep collagen using a water-soluble carbodiimide. Biomaterials 1996;17:765–73.

[27] Pieper JS, Hafmans T, Veerkamp JH, van Kuppevelt TH. Development of tailor-made collagen-glycosaminoglycan matrices: EDC/NHS crosslinking, and ultrastructural aspects. Biomaterials 2000;21:581–93.

[28] Wolf MT, Daly KA, Brennan-Pierce EP, Johnson SA, Carruthers CA, D'Amore A, et al. A hydrogel derived from decellularized dermal extracellular matrix. Biomaterials 2012;33:7028–38.

[29] Moody TP, Donovan MA, Laue TM. Turbidimetric studies of Limulus coagulin gel formation. Biophys J 1996;71:2012–21.

[30] Chernysh IN, Weisel JW. Dynamic imaging of fibrin network formation correlated with other measures of polymerization. Blood 2008;111:4854–61.

[31] Xiong JY, Narayanan J, Liu XY, Chong TK, Chen SB, Chung TS. Topology evolution and gelation mechanism of agarose gel . J Phys Chem B 2005;109:5638–43.

[32] Urry DW. Physical chemistry of biological free energy transduction as demonstrated by elastic protein-based polymers. J Phys Chem B 1997;101:11007–28.

[33] Yamaoka T, Tamura T, Seto Y, Tada T, Kunugi S, Tirrell DA. Mechanism for the phase transition of a genetically engineered elastin model peptide (VPGIG)(40) in aqueous solution. Biomacromolecules 2003;4:1680–5.

[34] Kinikoglu B, Rodríguez-Cabello JC, Damour O, Hasirci V. A smart bilayer scaffold of elastin-like recombinamer and collagen for soft tissue engineering. J Mater Sci Mater Med 2011;22:1541–54.

[35] Omidian H, Hasherni S, Askari F, Nafisi S. Swelling and crosslink density measurements for hydrogels. Iran J Polym Sci Technol 1994;3:115–9.

[36] Tibbitt MW, Kloxin AM, Sawicki LA, Anseth KS. Mechanical properties and degradation of chain and step- polymerized photodegradable hydrogels. Macromolecules 2013;46:2785–92.

[37] Liang H-C, Chang Y, Hsu C-K, Lee M-H, Sung H-W. Effects of crosslinking degree of an acellular biological tissue on its tissue regeneration pattern. Biomaterials 2004;25:3541–52.

[38] Costello LC, Franklin RB. A review of the important central role of altered citrate metabolism during the process of stem cell differentiation. J Regen Med Tissue Eng 2013;2:1.

[39] Keselowsky BG, Collard DM, García AJ. Integrin binding specificity regulates biomaterial surface chemistry effects on cell differentiation. Proc Natl Acad Sci U S A 2005;102:5953–7.

[40] Tanahashi M, Matsuda T. Surface functional group dependence on apatite formation on self-assembled monolayers in a simulated body fluid. J Biomed Mater Res 1997;34:305–15.

[41] Song J, Saiz E, Bertozzi CR. A new approach to mineralization of biocompatible hydrogel scaffolds: an efficient process toward 3-dimensional bonelike composites. J Am Chem Soc 2003;125:1236–43.

[42] Phadke A, Zhang C, Hwang Y, Vecchio K, Varghese S. Templated mineralization of synthetic hydrogels for bone-like composite materials: Role of matrix hydrophobicity. Biomacromolecules 2010;11:2060–8.

[43] Gomes S, Leonor IB, Mano JF, Reis RL, Kaplan DL. Spider silk-bone sialoprotein fusion proteins for bone tissue engineering. Soft Matter 2011;7:4964.

[44] Gungormus M, Branco M, Fong H, Schneider JP, Tamerler C, Sarikaya M. Self assembled bi-functional peptide hydrogels with biomineralization-directing peptides. Biomaterials 2010;31:7266–74.

Supplementary data

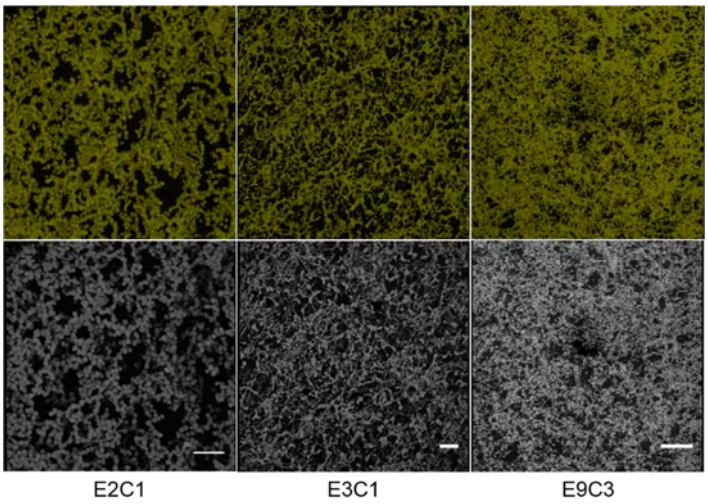

Fig. S1

Comparison of 3D reconstructions of calculated polymer-occupied volume (top) to 3D reconstructions of sections obtained by confocal microscopy (bottom). Scale bar: 20 µm.

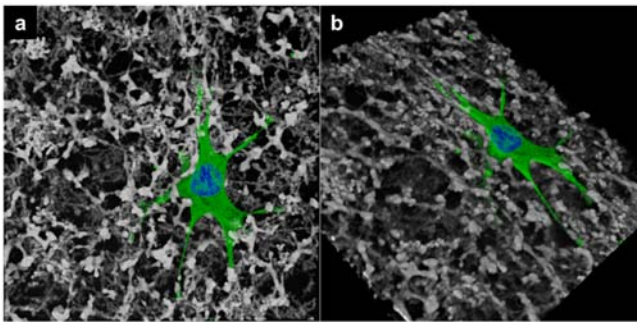

Fig. S2

(a) Front and (b) tilted view of a rMSC with filopodia entering a E3C1 hydrogel. Green: vinculin; blue: nuclei.